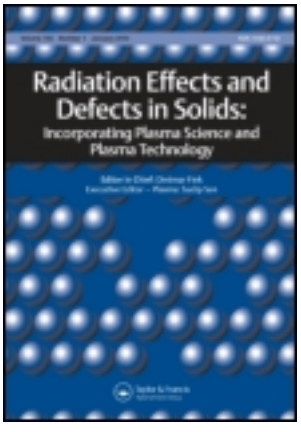

Radiation Effects and Defects in Solids: Incorporating Plasma Science and Plasma Technology

Publication details, including instructions for authors and subscription information:
http://www.tandfonline.com/loi/grad20

Studies on defect formation in femtosecond laser-irradiated PMMA and PDMS

K. L.N. Deepak [a] , R. Kuladeep [a] , S. Venugopal Rao [b] & D. Narayana Rao [a]

[a] School of Physics, University of Hyderabad, Hyderabad, 500046, India

[b] Advanced Centre of Research in High Energy Materials (ACRHEM), University of Hyderabad, Hyderabad, 500046, India

Available online: 01 Nov 2011

To cite this article: K. L.N. Deepak, R. Kuladeep, S. Venugopal Rao & D. Narayana Rao (2012): Studies on defect formation in femtosecond laser-irradiated PMMA and PDMS, Radiation Effects and Defects in Solids: Incorporating Plasma Science and Plasma Technology, 167:2, 88-101

To link to this article: http://dx.doi.org/10.1080/10420150.2011.620956

Radiation Effects & Defects in Solids
Vol. 167, No. 2, February 2012, 88–101

Taylor & Francis
Taylor & Francis Group

Studies on defect formation in femtosecond laser-irradiated PMMA and PDMS

K.L.N. Deepak[a], R. Kuladeep[a], S. Venugopal Rao[b] and D. Narayana Rao[a]*

[a]*School of Physics, University of Hyderabad, Hyderabad 500046, India;* [b]*Advanced Centre of Research in High Energy Materials (ACRHEM), University of Hyderabad, Hyderabad 500046, India*

(*Received 18 January 2011; final version received 1 September 2011*)

We report here our results on the spectroscopic and elemental analysis of femtosecond (fs) laser-modified regions in polymers of polymethylmethacrylate (PMMA) and polydimethylsiloxane (PDMS) in the context of defect formation and emission in the visible region. Different physical and chemical models are used to explain the changes in modified regions. We found that the emission intensity, recorded from the fs-modified regions of polymers, decreased over time to a constant value. We also demonstrate that these materials are suitable for the preparation of the microstructures en route for light guiding applications. The fs laser-irradiated regions exhibited paramagnetic behavior as was confirmed from electron spin resonance studies through the formation of peroxide-type free radicals. Raman mapping was performed in the modified regions which consisted of defects and found that the modulations in intensity are predominant in the central portion of the structure compared to edges. Elemental analysis has been performed in the modified regions using field emission scanning electron microscope instrument and energy-dispersive X-ray absorption spectroscopy to estimate the percentage contents of individual elements which resulted in defect formation such as paramagnetic and optical centers.

Keywords: femtosecond; polymers; FESEM; EDXAS; free radicals; optical centers; Raman mapping; emission

1. Introduction

Recent advances in ultrafast lasers have paved way for a variety of ultrafast sources with different pulse durations and energies making them an attractive tool for micromachining applications. The dominant mechanisms involved in ultrafast laser ablation are different from long-pulse ablation. While ablation, on a longer time scale (nanoseconds or longer), is reasonably well understood, the physics involved in ablation using short (ps, fs) pulses is yet to be entirely explored. Various relevant processes, both theoretical (*1–2*) and experimental (*3–5*), have been investigated in the past. Laser direct writing of microstructures within the bulk, and in a variety of materials including dielectrics, semiconductors, polymers, etc., has fascinated physicists and material scientists alike resulting in diverse applications. Higher order nonlinear optical processes are invoked at the focal volume when a femtosecond (fs) laser pulse is tightly focussed even in an optically transparent material. This leads to highly localized energy deposition and results in a range of changes in

*Corresponding author. Email: dnrsp@uohyd.ernet.in

ISSN 1042-0150 print/ISSN 1029-4953 online

http://dx.doi.org/10.1080/10420150.2011.620956
http://www.tandfonline.com

material properties. Fs laser direct writing (structures within the bulk) and fs micromachining (structures on the surface) have been demonstrated to be powerful microfabrication tools, whose applications are now established extensively in the fields of photonics, micro-/nano-fluidics and biology (*6–14*). Multi-photon absorption process which is involved and plays a major role in the interaction between the fs pulses and material occurs only in the vicinity of the focal spot, leaving the surface of the material intact. One of the most important applications of this ability to modify the refractive index (RI) is in the field of photonics and microfluidics (*15–19*). Therefore, it is imperative to completely understand the physical mechanisms occurring in the modified regions (within the bulk or surface) to develop superior photonic and microfluidic structures for practical device applications. Herein, we present our results on the studies of various structures fabricated with different writing conditions using ∼100 fs pulses and their spectroscopic and elemental characterizations.

2. Experimental details

Complete details of experimental setup can be found in our earlier publications (*20–23*). PMMA and PDMS with thicknesses of 1 and 6 mm were used in all our experiments. These samples are cut into 1 cm × 1 cm dimensions using polymer cutter and are polished, sonicated and dried before using for writing the structures. We have fabricated microstructures in PMMA (purchased from Goodfellow, USA) and home-made PDMS bulk polymers. In all the experiments, microstructures were fabricated using a Ti:sapphire oscillator-amplifier system operating at a wavelength of 800 nm delivering ∼100 fs, ∼1 mJ output energy pulses at a repetition rate of 1 kHz. Three translational stages (Newport) were arranged to translate the sample in X, Y and Z directions. Laser energy is varied using the combination of half wave plate and a polarizer. The writing was performed in the transverse geometry with polarization of the input beam perpendicular to the translation of the sample. We have used 40× microscope objective (numerical aperture (NA) of 0.65) in our experiments for focussing. The energies mentioned herewith were measured exactly after the laser excluding transmission and reflection losses.

3. Results and discussion

A 800 nm photon corresponds to 1.55 eV energy while the optical band gap of pure PMMA is 4.58 eV, implying that the nonlinear process involves at least three photons being responsible for structural modification at the focal volume (*24*). Figure 1(a) and (b) shows the chemical structure of PMMA and PDMS, respectively. Figure 1(c) and (d) shows the surface microstructures fabricated in PMMA using 640 nJ and 100 μJ energies with 1 mm/s speed using 40× objective lens. We clearly observed structures becoming smoother and narrower at lower irradiation intensities. These structures, fabricated at low energies, find applications in guiding light. There are three possible physical mechanisms (*9*) leading to ionization that are likely to occur when fs laser pulses interact with materials namely tunneling, intermediate and multi-photon ionizations. The Keldysh parameter was used to estimate the dominant ionization mechanism. Figure 2(a) shows the plot of the Keldysh parameter with peak intensities used to fabricate the surface structures in our experiments in PMMA. Keldysh parameter suggests that the dominant mechanism is tunneling ionization. Figure 2(b) shows the plot of structure width with energy. Lippert and Dickinson (*25*) have reported different theoretical chemical models to explain the ablation phenomena when materials, especially polymers, interact with laser pulses. The ablation mechanisms have been studied for more than two decades. As a result, the original strict separation of the models such as photochemical models by chemists and photothermal models by physicists is slowly blurring.

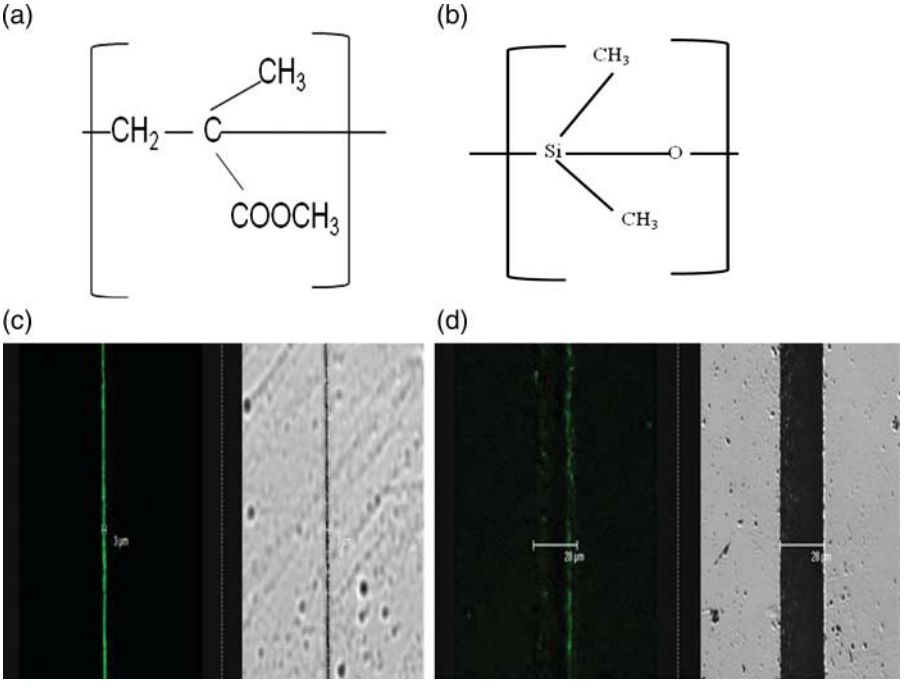

Figure 1. Chemical structure of (a) PMMA (b) PDMS surface structure fabricated in PMMA at (c) 640 nJ, 1 mm/s speed and 40× objective with width 3 μm (d) 100 μJ, 1 mm/s speed and 40× objective with width 28 μm.

Ablation can change the chemical and/or physical properties of the polymer resulting in modified chemical composition, altered optical absorption and electrical conductivity (*25*). Polymers consist of long molecular chains with strong covalent bonds binding the atoms and the monomers. At the same time, molecules belonging to different chains interact weakly. Therefore, a polymer material can be treated as a simple molecular solid. These long polymer chains can be broken into small pieces by direct photochemical effect (UV photons possess energy exceeding the energy of covalent bond). The absorbed energy provides a photochemical chain breaking. Thus, the model can be treated as photochemical. In the case of the photothermal model, the absorbed energy produces an elevated temperature high enough for the thermal destruction of the polymer (*25–28*). If the photons do not have sufficient energy to break covalent bonds, then the photothermal process occurs. Though the terms "photochemical" and "photothermal" are used to describe ablation, a microscopic description of the processes involved in each mechanism is lacking. In the experiment, clarifying such details is complicated because of the fact that plethora of experimental conditions and material properties (such as wavelength, fluence, pulse duration and absorption characteristics) can influence an assortment of different molecular events (*29*).

Several groups have reported fs laser-irradiated photo-modification of PMMA, where 800 nm excitation was used, conflicting with results about the sign of refractive index change. Negative Δn were found in the focal volume with an fs oscillator (25 MHz repetition rate) (*30*), whereas positive Δn were observed with 1 kHz regenerative amplifiers (*31*, *32*), indicating that the repetition rate influences the modification through thermal effects. Baum et al. (*19*) studied ultrashort-subablation threshold photo-modification effects at UV wavelengths (387 nm) in PMMA that has no linear absorption at this wavelength. They showed direct cleavage of the polymer backbone with the formation of monomers, leading to a change in the refractive index, Δn. In this way, one can expect that fs laser induced Δn in polymers leading to the photochemical process depending on the irradiation parameters resulting in positive or negative Δn (*33*). Photophysical model has both

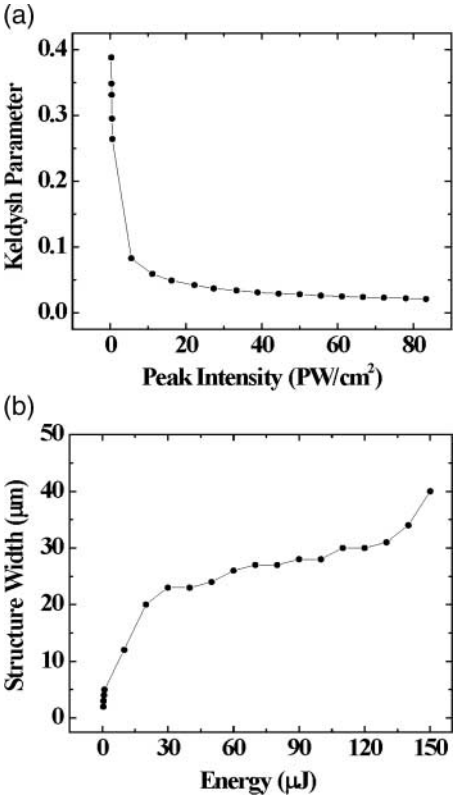

Figure 2. Plots of (a) the Keldysh parameter with different peak intensities of the pulses used for microfabrication and (b) structure width versus energy used for structures fabricated on the surface.

thermal and nonthermal processes playing an important role and this is most adequate for short laser pulses in the ps and fs ranges (*34*).

In the present work, we discuss the effects of photothermal model at different energies which are depicted in Figure 2(b). We had earlier reported (*22*) three different physical modifications to the material at different energies, namely, refractive index change (∼nJ), void formation (approximately few tens of μJ) and modification that includes void formation surrounded by refractive index change (hybrid type). In this paper, we report our studies on the refractive index change, which could be explained by the photochemical model and void formation, which could be explained by the photothermal model.

Earlier we had reported emission from the fs laser-modified regions of PMMA and PDMS (*22*). We observed this emission when excited at 458, 488 and 514 nm wavelengths in the case of PMMA and 543 and 633 nm wavelengths in the case of PDMS. There are sparse reports on the emission from photodegraded PMMA when it interacts with molecular oxygen (*35*). Nie et al. (*36–38*) have fabricated 3D fluorescent microcraters in PMMA and showed the possibility of using such fabricated structures toward memory-based devices. We observed a change in emission peak with different excitation wavelengths, suggesting the formation of different optical centers in polymers due to polymer chain scission upon fs laser irradiation, though the excitation spectra collected were the same (*39*, *40*). Reports on the formation of luminescent craters in polymers by our group and other materials find immense applications in memory-based devices (*41–43*). We collected emission over a period of time in these polymer materials immediately after irradiation and observed a decreasing trend in emission intensity over a period of time to almost constant value. Figure 3(a) shows a microstructure fabricated inside PMMA at 20 μJ energy and 1 mm/s speed. The width

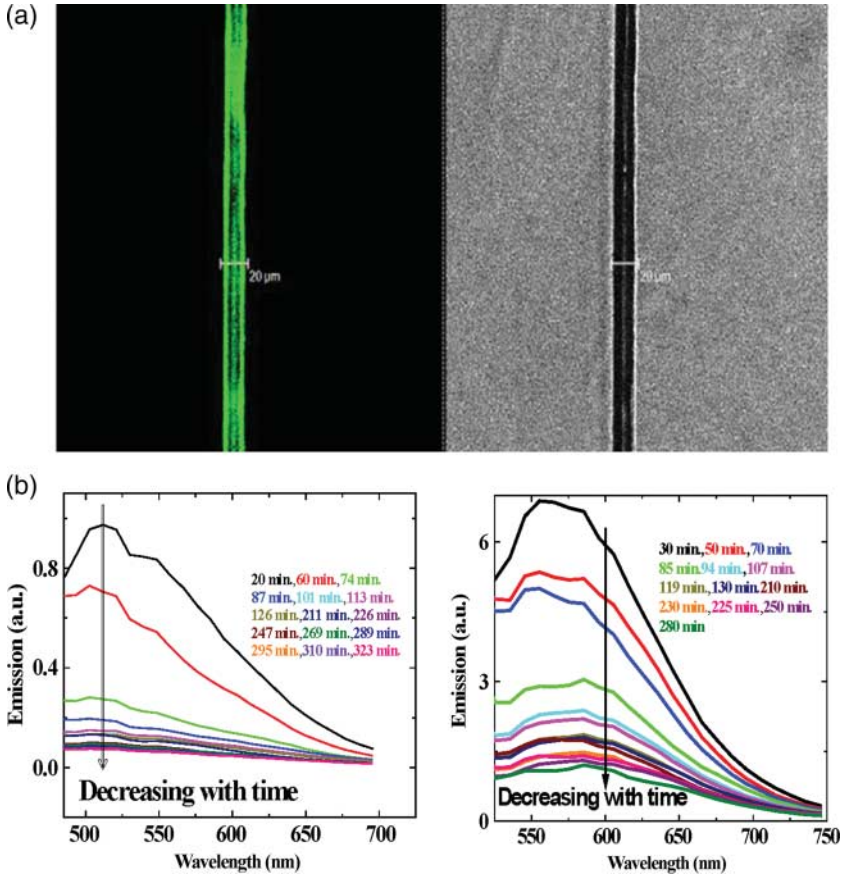

Figure 3. (a) Confocal microscope image of a structure fabricated inside PMMA 20 μJ energy, 1 mm/s speed and width = 20 μm. Pseudo-green color shows emission from the modified structure when excited at 488 nm. Time-dependent emission plots for excitation at (b) 458 nm and (c) 488 nm.

of the structure obtained from confocal microscopic studies is 20 μm. We observed pseudo-green color in the fs laser-modified region, which indicates the presence of emission. Moreover, we observed more green color at the edges compared with the central portion as the central portion of structure resulted in a void formation due to large intensities associated with the Gaussian pulse. Figure 3(b) and (c) shows the emission plots in PMMA with time excited at 458 and 488 nm wavelengths. Similar studies were carried out for PDMS also. A buried structure was fabricated in PDMS at 10 μJ energy with 1 mm/s speed as shown in Figure 4(a). The width of the structure fabricated was 18 μm. The pseudo-red color indicates the emission from the modified region excited at 633 nm. Figure 4(b) shows the plot of emission excited at 633 nm wavelength with time.

We reported several such structures fabricated in achieving microfluidic channels and gratings (*20–23*, *39*, *40*). Figure 5(a) and (b) shows the branched surface structures such as 1:8 splitter fabricated in PMMA and PDMS. Figure 5(c) shows the buried double Y waveguide fabricated in PMMA. There are two possible mechanisms for guiding light in these fs-fabricated structures. In the first case, low input energies create a positive refractive index change in the modified regions, thereby permitting to guide light in single Y coupler structures. In the second case, high input energies result in void formation and therefore the unmodified region in the middle of two modified structures can guide the light. If materials exhibit a negative refractive index change, then double structures like double waveguides and double Y couplers meet the requirements of

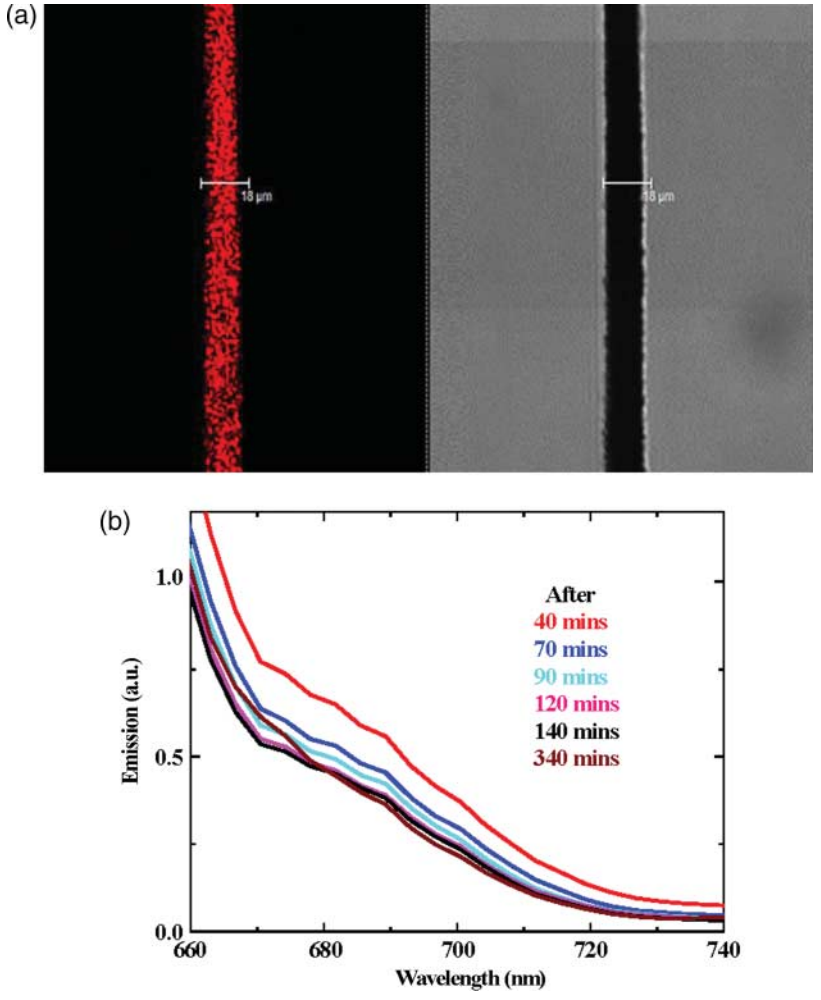

Figure 4. (a) Confocal microscope image of a microstructure fabricated inside PDMS at 10 μJ energy, 1 mm/s speed and width 18 μm. (b) Time-dependent emission plot for excitation at 633 nm wavelength.

wave guiding applications. All these structures showed pseudo-green color emission in the fs laser-modified regions.

We also present the data obtained through Raman mapping technique for a surface structure fabricated in PDMS (15 μJ energy, 0.05 mm/s speed). Our earlier studies showed broadening and suppression of Raman modes for the structures fabricated at high energies (*22*). Figure 6(a) shows the region of 50 μm over which the mapping was performed in steps of 1 μm (the portion of single structure of Figure 6(a)). The two peaks at 2904 and 2963 cm^{-1} correspond to CH_3 symmetric and asymmetric stretching modes (*44*) as shown in Figure 1(b). It clearly shows lower Raman intensity at central regions compared with the regions near the edges with slight broadening in the middle portion of the structure. We have also confirmed that in the case of voids, these modes completely disappear. Since these structures were fabricated using Gaussian pulses, portions of the structures modified by the central portion of the Gaussian pulse got modified to a maximum extent due to large intensities associated within the center of the pulse. Hence, there is slight broadening in the middle region compared to the edges. Figure 6(b) shows Raman mapping plot. Figure 6(c) shows how the Raman intensity behavior in 50 μm fs exposed region as the region experiences different amount of stress in various places.

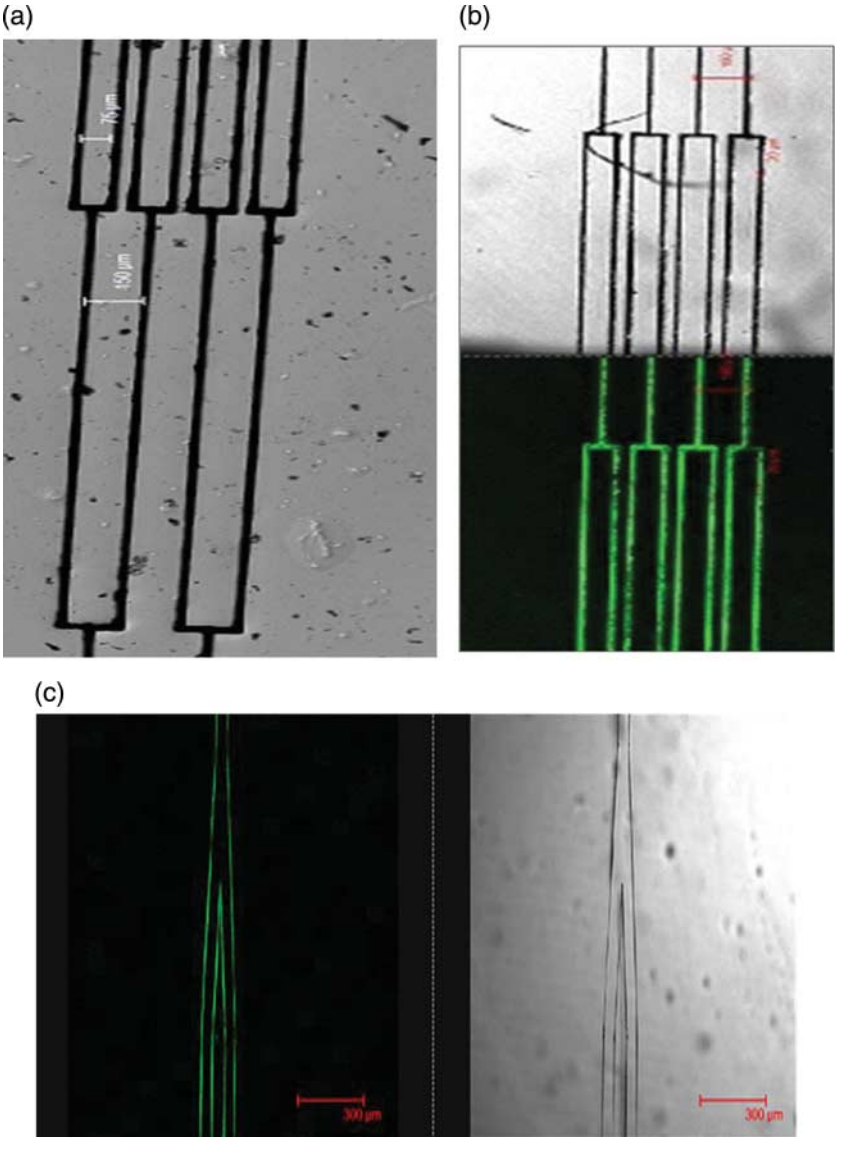

Figure 5. Confocal microscope image of (a) a branched surface structure (1:8 splitter) in PDMS (15 μJ and 0.05 mm/s speed, width 50 μm) and (b) (color online) 1:8 splitter on the surface of PMMA (15 μJ with 0.05 mm/s). Pseudo-green color represents emission when excited at 488 nm. Since the image is large, a part of the structure is shown. (c) (color online) Double Y coupler fabricated inside PMMA with 1 μJ energy, 1 mm/s speed. Pseudo-green color represents emission when excited at 488 nm. Pseudo-green color represents emission when excited at 488 nm. Since the image is large, a part of the structure is shown.

Though we predicted earlier (*22*) the peroxide-type free radicals in PMMA, we could not perform a detailed electron spin resonance (ESR) analysis. We reported the presence of same peroxide-type free radicals in PDMS. In this paper, we report the presence of peroxide-type free radicals in PMMA also. We could not observe these free radicals earlier in PMMA because the lifetime of these radicals in PMMA is nearly a day unlike in PDMS whose lifetime is more than 6 months. Nie et al. (*36*) have reported the observation of a nine-line spectrum in irradiated PMMA. There are reports on nine-line spectrum ESR of irradiated PMMA where irradiation is performed under 77 K. Szocs (*45*) had shown the same characteristic nine-line ESR spectrum

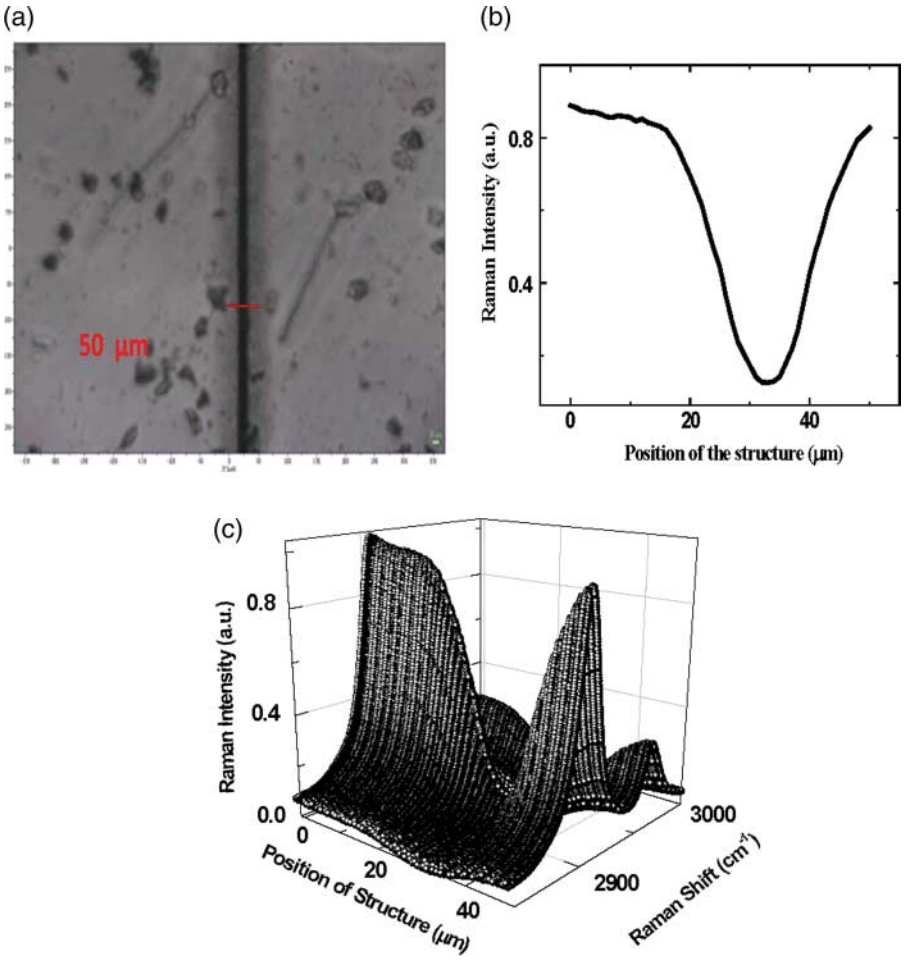

Figure 6. (a) Microscope image of the surface structure in PDMS fabricated using 15 μJ energy, 0.05 mm/s speed (scale bar: 50 μm). (b) Raman intensity versus position of the structure. (c) Raman mapping plot of the PDMS structure.

when irradiated with X-rays . Michel et al. (*46*) have systematically studied the photodegradation in PMMA using the ESR spectrometer. We irradiated PMMA under room temperature conditions and show peroxide-type free radicals in irradiated PMMA. Figure 7 shows the ESR signal collected from the fs-modified regions of PMMA. We observed the existence of peroxide radicals even at 1 μJ energy and below also. We predict that the difference in lifetimes could be due to the different host environments as shown in Figure 1(a) and (b).

In our endeavor to understand the composition after the polymer chain scission due to radiation effects that resulted in possible defect formation, we collected the field emission scanning electron microscope (FESEM) and energy-dispersive X-ray absorption spectroscopy (EDXAS) data from the fs laser-irradiated PMMA and PDMS. The main elements in PMMA are carbon (C) and oxygen (O), whereas for PDMS the main elements are silicon (Si), carbon (C) and oxygen (O). Since these structures were fabricated on the surface of these polymers, the ablated materials consisting of different compositions and main elements cannot escape anywhere but settle at the edges of the structures. Hence, there will be a variation in weight percentage/atomic percentage of these elements compared with pristine regions. Initially, we fabricated different microstructures on the surface of PMMA at 50, 40, 30, 20 and 10 μJ energies with 1 mm/s scanning speed. Figure 8(a) shows FESEM images of microstructures fabricated on the surface of PMMA. We

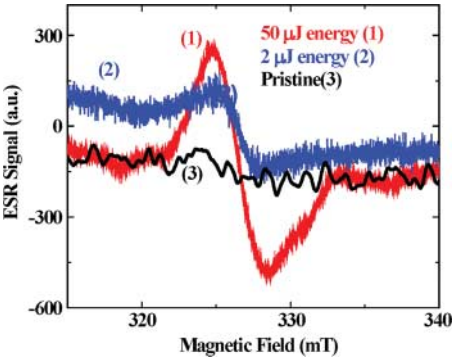

Figure 7. ESR signal in the case of irradiated PMMA at 50 and 2 μJ energies and 1 mm/s speed that exhibited paramagnetic behavior.

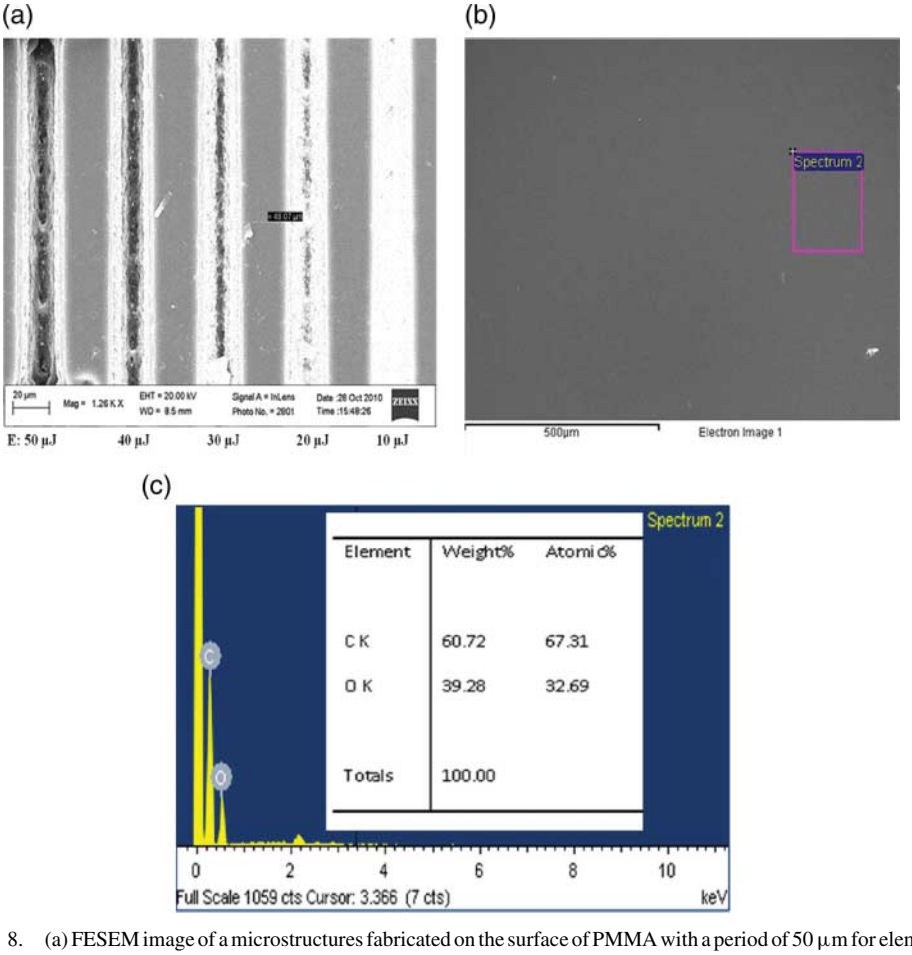

Figure 8. (a) FESEM image of a microstructures fabricated on the surface of PMMA with a period of 50 μm for elemental analysis using EDXAS. Energies of the fabricated structures are clearly mentioned below the picture. (b) Pristine region of PMMA where EDXAS is performed. (c) Percentage of various elements of carbon and oxygen in pristine PMMA.

observed void-type regions at the center from FESEM pictures for all the irradiation energies above 10 μJ. Figure 8(b) and (c) shows the pristine region of PMMA and the plot that shows percentage of elements present through EDXAS analysis. In EDXAS plots we present the elemental analysis data corresponding to the region highlighted by rectangular boxes in FESEM pictures. These

boxes indicate the regions of interest where EDXAS analysis has been performed to estimate percentage contents of the elements.

Several technological applications are found for the laser written structures (*6–14*). SEM pictures suggest a surface roughness of 1.5 μm through a single scan and this could be improved to 0.8 μm by repetitive scans. We also feel that further improvements could be achieved if our present system is mounted on vibrational isolation legs and the structures are written in a liquid

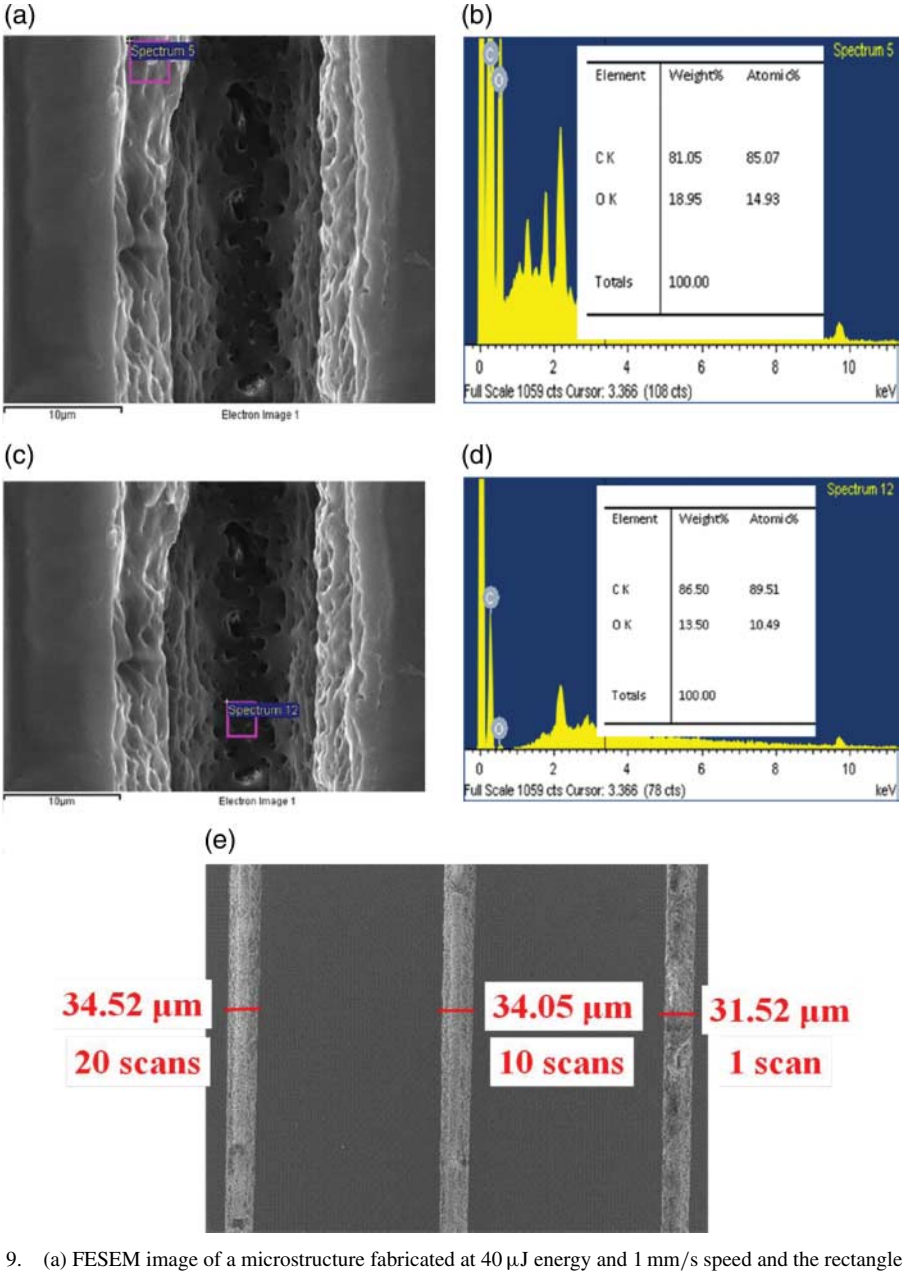

Figure 9. (a) FESEM image of a microstructure fabricated at 40 μJ energy and 1 mm/s speed and the rectangle shows the region where EDXAS is collected (scale bar: 10 μm). (b) Percentage contents of C and O in the end region. (c) The middle portion of the structure where EDAX is performed (scale bar: 10 μm). (d) The % contents of C and O. (e) SEM picture of fabricated structures on the surface of PMMA through single and multiple scans.

environment or treated with a liquid. Moreover, the surface wettability of polymers and their dependence on the roughness has been well studied (*47*, *48*), where a contact angle of 110° is shown for a surface roughness of 1.4 μm on a PMMA film. Figure 9 shows the SEM pictures and EDXAS data for the structures written on PMMA.

Figure 9(a) shows the modified region with average energy pulses of 40 μJ, 1 mm/s speed. Figure 9(b) shows the plot of percentage of elements. The weight percentage of C and O are 60 and 40 in pristine regions. The percentage of C and O found to be are 81 and 19 in the end regions. This is due to the settling of the ablated material from the modified regions as can be observed in FESEM pictures. In the case of middle portion of the structure, the percentage contents of C and O are 87 and 13, respectively. As the middle portion of the structure is influenced by higher intensities, one would expect material getting carbonized completely and hence there is a slight enhancement in the percentage of C. This is illustrated in the Figure 9(c) and (d). Figure 9(e) compares single and multiple scans.

Extending the same elemental analysis to PDMS, we focussed our attention to elements C, O and Si from Figure 1(b). For pristine regions of PDMS, we found the contents of C, O and Si in the percentage weight ratios of 26, 40 and 34, respectively. Figure 10(a) and (b) shows FESEM and EDXAS pictures. Figure 10(c) and (d) shows the FESEM picture of a microstructure on the surface

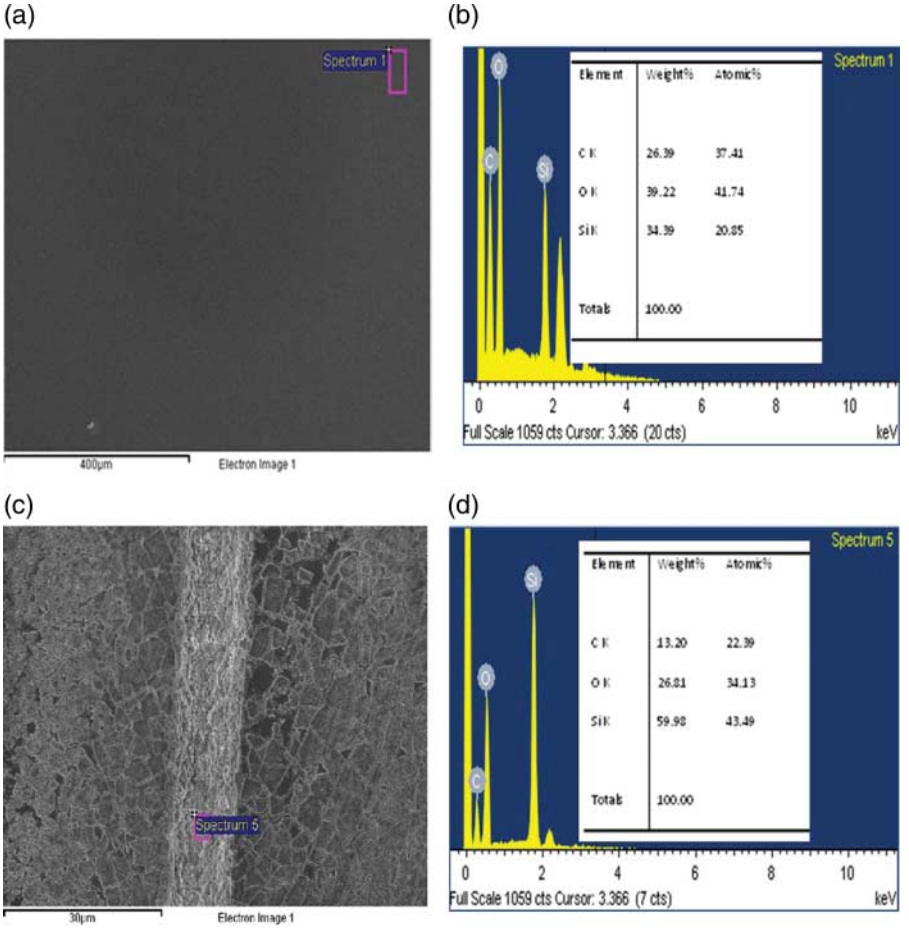

Figure 10. (a) FESEM image of a microstructure fabricated at 40 μJ energy and 1 mm/s speed and the rectangle shows the region where EDXAS is collected. (b) Percentage contents of C and O and Si in the pristine region. (c) The middle portion of the structure where EDXAS is performed (scale bar: 30 μm). (d) The percentage contents of C, O and Si.

of PDMS fabricated at 40 μJ energy with 1 mm/s scanning speed and weight percentage contents of different elements in the middle portion of the structure obtained with EDXAS analysis. We found the weight percentage of these elements to be 13, 27 and 60. Figure 10(c) and (d) shows the middle portion of the structure fabricated and EDXAS analysis. There is a slight decrement in carbon and oxygen elements unlike silicon, whose percentage content is increased. We found a similar trend in other cases that include at different regions of interest with different energies. Silicon is a heavier element compared with carbon and oxygen and hence it may not escape from the same regions.

Tables 1 and 2 show the weight percentage of different elements in PMMA and PDMS obtained with fs laser irradiation. We observed that for the structure fabricated at 1 μJ energy the percentage composition of C, O and Si showed no difference between end and central regions (Table 2). As the structure is narrow due to low-energy irradiation dose, there is not much appreciable gap left between end and middle regions. Also from the data presented in Tables 1 and 2, we could not establish a particular trend due to the complexity involved in the problem. At higher energies, we observed the ablated material getting settled on microscope objective that leads to the loss of the material, which cannot be accounted for the analysis part to study the distribution of various elements after fs laser treatment. Moreover, there could be a decrease in the irradiation energy as the settled ablated material on the microscope objective does not transmit all the light and lead to losses.

The percentage compositions of different elements in these fs laser-modified regions need further investigations to understand the fs ablation dynamics. Our future investigations are to

Table 1. Weight % of elements C and O at different energies in PMMA collected in different regions using EDXAS analysis.

S. no.	Energy (μJ)	Region	% C (% weight)	% O (% weight)
1	Pristine		61 ± 2	38 ± 2
2	50	End	71 ± 2	28 ± 2
		Middle	81 ± 2	18 ± 2
3	40	End	83 ± 2	16 ± 2
		Middle	85 ± 2	14 ± 2
4	30	End	82 ± 2	18 ± 2
		Middle	79 ± 2	21 ± 2
5	20	End	74 ± 2	26 ± 2
		Middle	88 ± 2	12 ± 2
6	10	End	80 ± 1	19 ± 1
		Middle	87 ± 1	12 ± 1

Table 2. Weight % of elements C, O and Si at different energies in PDMS collected in different regions using EDXAS analysis.

S. no.	Energy (μJ)	Region	% C (% weight)	% O (% weight)	% Si (% weight)
1	Pristine		28 ± 2	40 ± 1	32 ± 2
2	50	End	21 ± 3	25 ± 3	55 ± 1
		Middle	32 ± 1	22 ± 1	45 ± 1
3	40	End	8 ± 1	12 ± 2	78 ± 3
		Middle	13 ± 1	28 ± 2	56 ± 3
4	10	End	12 ± 1	22 ± 2	63 ± 1
		Middle	14 ± 1	19 ± 1	67 ± 1
5	1	End	24 ± 1	31 ± 1	45 ± 1
		Middle	24 ± 1	31 ± 1	45 ± 1

understand the ablation dynamics and the change in the percentage composition of different elements after fs laser treatment. This study will be useful in analyzing the spectroscopic properties of the modified regions to explain the changes observed through confocal micro-Raman, ESR and absorption and fluorescence spectroscopic techniques.

We are also focussing our studies on the analysis of the formation of different optical centers after fs laser treatment and time-dependent emission behavior. We are also investigating the various mechanisms involved in the formation of free radicals that exhibit paramagnetic behavior.

4. Conclusions

In this work, we report a shift in the emission peak with different excitation wavelengths in the case of fs-modified PMMA and PDMS, which indicates the formation of different optical centers and/or defects generated through fs laser irradiation. We also observed emission intensity maximum in these polymers PMMA and PDMS initially after fabrication and decreased to a constant value with time. 1:8 beam splitter and double Y couplers were used to demonstrate and achieve wave guiding in near future. Raman mapping technique performed across a microstructure in PDMS showed maximum stress in the middle due to large intensities associated with the central portion of the fs laser pulse. ESR showed the existence of peroxide-type free radicals in PMMA and PDMS. However, lifetimes of these radicals were found to be different with 1 day for PMMA and more than 6 months for PDMS. SEM and EDXAS were performed on the surface structures of PMMA and PDMS to understand the redistribution of different elements resulting from fs laser irradiation which leads to the formation of optical centers and/or defects and free radicals.

Acknowledgements

K.L.N. Deepak acknowledges the senior research fellowship from Council of Scientific and Industrial Research (CSIR), India. D.N.R. and S.V.R. acknowledge the financial support from the CSIR and Department of Science and Technology.

References

(1) Jeschke, H.; Garcia, M.; Lenzer, M.; Bonse, J.; Kruger, J.; Kautek, W. *Appl. Surf. Sci.* **2002,** *197–198,* 839–844.
(2) Lorazo, P.; Lewis, L.; Meunier, M. *Phys. Rev. Lett.* **2003,** *91,* 225502-1–225502-4.
(3) Pronko, P.; VanRompay, P.; Horvth, C.; Loesel, F.; Juhasz, T.; Liu, X.; Mourou, G. *Phys. Rev. B*. **1998,** *58,* 2387–2390.
(4) Borowiec, A.; MacKenzie, M.; Weatherly, G.; Haugen, H. *Appl. Phys. A*. **2003,** *76,* 201–207.
(5) Bonse, J.; Brzezinka, K.-W.; Meixner, A.J. *Appl. Surf. Sci.* **2004,** *221,* 215–230.
(6) Davis, K.M.; Miura, K.; Sugimoto, N.; Hirao, K. *Opt. Lett.* **1996,** *21,* 1729–1731.
(7) Marcinkevicius, A.; Juodkazis, S.; Watanabe, W.; Miwa, M.; Matsuo, S.; Misawa, H.; Nishii, J. *Opt. Lett.* **2001,** *26,* 277–179.
(8) Nasu, Y.; Kohtoku, M.; Hibino, Y. *Opt. Lett.* **2005,** *30,* 723–725.
(9) Schaffer, C.B.; Brodeur, A.; Mazur, E. *Meas. Sci. Technol.* **2001,** *12,* 1784–1794.
(10) Gattass, R.R.; Mazur, E. *Nat. Photonics* **2008,** *2,* 219–225.
(11) Mézel, C.; Bourgeade, A.; Hallo, L. *Phys. Plasmas* **2010,** *17,* 113504–113520.
(12) Wang Z.K.; Zheng H.Y.; Xia H.M. *Microfluid Nanofluid*, **2011,** 10, 225.
(13) Zhang, Y.-L.; Chen, Q.-D.; Xia, H.; Sun, H.-B. *Nano Today* **2010,** *5,* 435–448.
(14) Lee, C.-Y.; Chang, T.-C.; Wang, S.-C.; Chien, C.-W.; Cheng, C.-W. *Biomicrofluidics* **2010,** *4,* 046502–046506.
(15) Homoelle, D.; Wielandy, S.; Gaeta, A.L.; Borrelli, N.F.; Smith, C. *Opt. Lett.* **1999,** *24,* 1311–1313.
(16) Li, Y.; Watanabe, W.; Yamada, K.; Shinagawa, T.; Itoh, K.; Nishii, J.; Jiang, Y. *Appl. Phys. Lett.* **2002,** *80,* 1508–1510.
(17) Chan, J.W.; Huser, T.R.; Risbud, S.H.; Hayden, J.S.; Krol, D.M. *Appl. Phys. Lett.* **2003,** 82, 2371–2373.
(18) Minoshima, K.; Kowalevicz, A.M.; Hartl, I.; Ippen, E.P.; Fujimoto, J.G. *Opt. Lett.* **2001,** *26,* 1516–1518.
(19) Baum, A.; Scully, P.J.; Basanta, M.; Thomas, C.L.P.; Fielden, P.R.; Goddard, N.J.; Perrie, W.; Chalker, P.R. *Opt. Lett.* **2007,** *32,* 190–192.
(20) Vishnubhatla, K.C.; Venugopal Rao, S.; Sai Santosh Kumar, R.; Shiva Prasad, K.; Prasad, P.S.R.; Narayana Rao, D. *Opt. Commun.* **2009,** *282,* 4537–4542.

(21) Vishnubhatla, K.C.; Venugopal Rao, S.; Sai Santosh Kumar, R.; Osellame, R.; Bhaktha, S.N.B.; Turrell, S.; Chiappini, A.; Chiasera, A.; Ferrari, M.; Mattarelli, M.; Montagna, M.; Ramponi, R.; Righini, G.C.; Narayana Rao, D. *J. Phys. D.: Appl. Phys.* **2009,** *42,* 205106–205112.
(22) Deepak, L.N.K.; Narayana Rao, D.; Venugopal Rao, S. *Appl. Opt.* **2010,** *49,* 2475–2489.
(23) Deepak, K.L.N.; Venugopal Rao, S.; Narayana Rao, D. *Pramana* **2010,** *75,* 1221–1232.
(24) Baum, A.; Scully, P.J.; Perrie, W.; Jones, D.; Issac, R.; Jaroszynski, D.A. *Opt. Lett.* **2008,** *33,* 651–653.
(25) Lippert, T.; Dickinson, J.T. *Chem. Rev.* **2003,** *103,* 453–485.
(26) Bityurin, N.; Lukyanchunk, B.S.; Hong, M.H.; Chong, T.C. *Chem. Rev.* **2003,** *103,* 519–552.
(27) Lippert, T. *Plasma Process Polym.* **2005,** *2,* 525–546.
(28) Srinivasan, R.; Braren, B.; Casey, K.B. *Pure Appl. Chem.* **1990,** *62,* 1582–1584.
(29) Patrick, F.C.; Prasad, M.; Barabara, J.G. *Acc. Chem. Res.* **2008,** *41* (8), 915–924.
(30) Zoubir, A.; Lopez, C.; Richardson, M.; Richardson, K. *Opt. Lett.* **2004,** *29,* 1840–1842.
(31) Wochonowiski, C.; Cheng, Y.; Meteva, K.; Sugioka, K.; Midorikawa, K.; Metev, S. J. *Opt. A* **2005,** *7,* 493–501.
(32) Sowa, S.; Watanabe, W.; Tamaki, T.; Nishii, N.; Itoh, K. *Opt. Express* **2006,** *14,* 291–297.
(33) Della Valle, G.; Osellame, R.; Laporta, P. *J. Opt. A: Pure Appl. Opt.* **2009,** *11,* 013001–013018.
(34) Bityurin, N.; Malyshev, A.; Lukyan Chuk, B.; Anisimov, S.; Bauerle, D. *Proc. SPIE* **1996,** *2802,* 103–112.
(35) Dickens, B.; Martin, J.W.; Waksman, D. *Polymer* **1984,** *25,* 706–715.
(36) Nie, Z.; Lee, H.; Yoo, H.; Lee, Y.; Kim, Y.; Lim, K.-S.; Lee, M. *Appl. Phys. Lett.* **2009,** *94,* 111912–111914.
(37) Nie, Z.; Lim, K.-S.; Lee, H.; Lee, M.; Kobayashi, T. *J. Lumin.* **2011,** *131,* 266–270.
(38) Nie, Z.G.; Lim, K.-S.; Jang, W.Y.; Lee, H.Y.; Lee, M.K.; Kobayashi, T. *J. Phys. D: Appl. Phys.* **2010,** *43,* 485101–485106.
(39) Deepak, K.L.N.; Kuladeep, R.; Venugopal Rao, S.; Narayana Rao, D. *Chem. Phys. Lett.* **2011,** *503,* 57–60.
(40) Deepak, K.L.N.; Kuladeep, R.; Praveen Kumar, V.; Venugopal Rao, S.; Narayana Rao, D. *Opt. Commun.* **2011,** *284,* 3074–3078.
(41) Watanabe, M.; Juodkazis, S.; Sun, H.-B.; Matsuo, S.; Misawa, H. *Phys. Rev. B* **1999,** *60,* 9959–9964.
(42) Kudrius, T.; Slekys, G.; Juodkazis, S. *J. Phys. D.: Appl. Phys.* **2010,** *43,* 145501–145505.
(43) Hongfang, J.; Lixin, Z. *J. Rare Earths* **2009,** *27* (5), 786–789.
(44) Bae, S.C.; Lee, H.; Lin, Z.; Granick, S. *Langmuir* **2005,** *21,* 5685–5688.
(45) Szocs, F. *Chem. Papers* **1999,** *53* (2), 137–139.
(46) Michel, R.E.; Chapman, F.W.; Mao, T.J. *J. Chem. Phys.* **1966,** *45* (12), 4604–4611.
(47) Nathawat, R.; Kumar, A.; Acharya, N.K.; Vijay, Y.K. *Surf. Coat. Technol.* **2009,** *203,* 2600–2604.
(48) De Marco, C.; Eaton, S.M.; Suriano, R.; Turri, S.; Levi, M.; Ramponi, R.; Cerullo, G.; Osellame, R. *ACS Appl. Mater. Interfaces* **2010,** *2,* 2377–2384.